Water Dipole Populations in the Electrical Double Layer and Their Contributions to the Total Interfacial Potential at Different Surface Charge Densities

Benjamin Rehl,[a] *Emily Ma,*[b] *Shyam Parshotam,*[a] *Emma L. DeWalt-Kerian,*[a] *Tianli Liu,*[a] *Franz M. Geiger,*[*,b] *and Julianne M. Gibbs*[*,a]

[a]Department of Chemistry, University of Alberta, Edmonton, Alberta, T6G 2G2, Canada

[b]Department of Chemistry, Northwestern University, Evanston, Illinois 60208, USA

Abstract: The electric double layer governs the processes of all charged surfaces in aqueous solutions, however elucidating the structure of the water molecules is challenging for even the most advanced spectroscopic techniques. Here, we present the individual Stern layer and diffuse layer OH stretching spectra at the silica/water interface in the presence of NaCl over a wide pH range using a combination of vibrational sum frequency generation and heterodyned second harmonic generation techniques, streaming potential measurements, and the maximum entropy method. We find that the Stern layer water molecules and diffuse layer water molecules respond differently to pH changes: unlike the diffuse layer, whose water molecules remain net-oriented in one direction, water molecules in the Stern layer flip their net orientation as the solution pH is reduced from basic to acidic. We obtain an experimental estimate of the dipole potential contribution to the total potential drop across the insulator/electrolyte interface and find it to

dominate over the Coulomb-only (Gouy-Chapman, Gouy-Chapman-Stern) contribution. We quantify how these contributions result in a considerable influence on the vibrational lineshapes. Our findings show that a purely Coulombic view is insufficient to accurately describe the electrical double layer over aqueous interfaces.

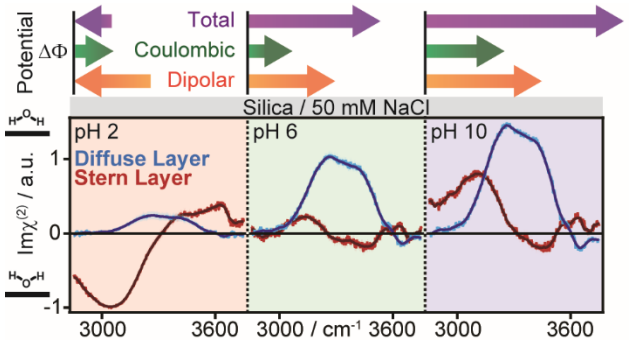

Introduction. The electrical double layer (EDL) over charged aqueous interfaces is commonly described[1-2] using theories going back to Helmholtz,[3] Gouy,[4] Chapman,[5] Stern,[6] and Grahame.[7] These mean field approximations account for the distribution of ions in close proximity to the surface and those further away in the diffuse layer, but do not include the molecular structure and chemical identity of the species comprising the EDL. Moreover, these models provide a purely Coulombic view that is based on the Poisson solution of mobile, free point charges over a uniformly charged and infinitely thin plane. Dipolar, quadrupolar, and other non-Coulombic contributions to the total potential drop across the interface are neglected, even though increasing evidence from experiment and theory points to their substantial contributions to the total interfacial potential.[8-17] Therefore, our current understanding of the EDL needs to be improved by considering electrostatic potential contributions beyond Coulomb-only terms. In addition, while the structure of some ions in the EDL are well understood from various measurements,[18-21] the way water molecules (dipoles) orient and network themselves in its two main structural features, the Stern layer and the diffuse layer, remains enigmatic.

Strategies have evolved to address these shortcomings, such as potentiometric titrations,[20] electrical impedance measurements,[22-23] ion adsorption batch experiments,[19, 21] or electrokinetic and electrophoretic techniques,[24-25] with subsequent data interpretation employing surface complexation models.[26-27] Other methods include atomic force microscopy (AFM),[28-29] X-ray spectroscopies like X-ray standing wave and X-ray reflectivity measurements,[18, 30-31] and vibrational sum frequency generation spectroscopy.[32-34] Employing ultraflat boehmite, AFM has recently been used to report directly on the interfacial water structure[35] that constitutes the greatest component of the EDL. X-ray reflectivity and spectroscopy measurements have yielded the position of ions and hydration layers[26, 36] in the EDL for a number of different mineral oxides

including mica,[37-40] titania,[26, 41] alumina,[36] and quartz.[42-43] More recently, X-ray photoelectron spectroscopy of colloidal dispersions in a microjet were used to obtain estimates for the surface potential as a function of ion concentration and identity,[18] which was used in conjunction with electrokinetic measurements to infer the thickness of the Stern layer.[44]

Despite these important advances, information on the orientation of water molecules, their hydrogen bonding strength and resulting dipole and higher-order electrostatic potentials in the EDL is still lacking. Furthermore, owing to the challenges associated with these experiments, measurements are generally performed at only one or a few pH values and a limited ionic strength range. As pH determines the surface charge density and interfacial potentials over amphoteric oxides such as silica, it would be ideal to monitor how the structure of the EDL evolves under a range of pH conditions. Measuring the hydrogen-bonded structure of water and its absolute orientation in the Stern and the diffuse layers would provide highly complementary information to that from X-ray and scanning probe measurements, bringing us closer to the goal of generating a complete molecular picture of charged aqueous interfaces.[34, 39]

Vibrational sum frequency generation (SFG) spectroscopy is intrinsically sensitive to non-centrosymmetric assemblies of oscillators. Consequently, the technique has been extensively used to measure the interfacial regions of charged surfaces and aqueous solutions.[32-34] In principle, these studies can offer a wealth of chemical information such as bond strength, including hydrogen bond strength, and molecular orientation of the net assembly of water. However, vibrational SFG spectroscopy convolutes the depth dependence of the bulk and interfacial SFG signal sources, which is especially problematic in the presence of non-zero surface potentials. Specifically, the wave vector mismatch for the reflection geometries commonly used in most SFG setups is on the

order of 10^7 m^{-1}, leading to third-order (bulk allowed) contributions that add to the second-order (interface-specific) SFG response depending on the interfacial potential.[45-51]

While it has been known for a while how these second- and third-order contributions are encoded in the total detected SFG signal,[52-53] the proper lineshape analysis requires knowledge of the phase relationship between these two terms and the total interfacial potential, which has remained elusive. To overcome this problem, we now combine vibrational sum frequency and non-resonant second harmonic generation (SHG) measurements to obtain the interface-specific response for the fused silica/water interface as a function of pH and a total ionic strength of 50 mM. In addition to obtaining the total potential drop across the fused silica/water interface using heterodyne-detected SHG spectroscopy, we disentangle the bulk and surface contributions in our vibrational SFG lineshapes that arise from absorptive-dispersive mixing. Together with streaming potential measurements, our approach enables us to elucidate the net orientation of tight and loose hydrogen bond networks in the Stern layer over fused silica for a range of bulk solution pH conditions at a constant ionic strength of 50 mM NaCl. We identify conditions where interfacial water molecules held in a tight hydrogen bonded network flip their net orientation with pH, while observing no such flip in the diffuse layer. As such, we attribute the non-monotonic trend in the overall SFG intensity spectra with decreasing pH to changes in the water structure at the surface rather than changes in the diffuse layer structure. Together with the observed streaming potentials, we find an important role of dipole potential contributions to the total interfacial potential on top of the Coulomb-only contributions. We thus provide new physical insights for charged solid/aqueous interfaces that hold the promise of developing our understanding of the EDL beyond mean field theories.

Results and Discussion.

Nonlinear Optics and Electrokinetics in the Electrical Double Layer. The intensity in our vibrational SFG spectra originates from water molecules located in environments that lack inversion symmetry. The centrosymmetry of bulk water is broken in the electrical double layer by four phenomena: hydrogen bonding of water molecules with the underlying surface, the ordering of water around specifically and non-specifically adsorbed ions, the alignment of water permanent dipoles with the electric field emanating from charged sites at the surface, and the polarization of water molecules in said field. The first (hydrogen bonding with the surface) is expected to be largely responsible for the water structure in the Stern layer,[47-48, 54] which we attribute to the second-order susceptibility $\chi_S^{(2)}$. The SFG intensity is then given by the following equation:

$$I_{\mathrm{SFG}} \propto \left|\chi_{\mathrm{total}}^{(2)}\right|^2 = \left|\chi_S^{(2)} + \chi_{DL}^{(2)}\right|^2 \qquad \text{eq. 1}$$

Here, I_{SFG} is the intensity of sum frequency light, and $\chi_{\mathrm{total}}^{(2)}$, $\chi_S^{(2)}$, and $\chi_{DL}^{(2)}$ are the total, Stern layer, and diffuse layer second-order susceptibilities, respectively. For our SFG measurements, $\chi_S^{(2)}$ describes the vibrations of all OH oscillators within the Stern layer and is dependent on the number and net orientation of these oscillators. The Stern layer thickness, and therefore the number of contributing water molecules, is intrinsically coupled to the ionic strength of the aqueous solution according to a recent XPS report of Stern layer compression with increasing salt concentration.[44] The region of aligned and polarized water molecules outside of the Stern layer is called the diffuse layer, which we quantify in equation 1 with the $\chi_{DL}^{(2)}$ term, according to

$$\chi_{DL}^{(2)} = \chi^{(3)} \int_{\mathrm{OHP}}^{\infty} \mathrm{E_0(z)} \mathrm{e}^{\mathrm{i}\Delta \mathrm{kz}} \mathrm{dz} \qquad \text{eq.2}$$

Here, $E_0(z) = -\frac{d\Phi(z)}{dz}$ is the electric field emanating from the surface which is integrated from the plane marking the end of the Stern layer, the outer Helmholtz plane (z = OHP), to infinite distance from the interface ($\Phi(z = \infty) = 0$ V) to yield the absolute value and sign of the OHP electrostatic potential Φ_{OHP}. The OHP potential is often approximated as the zeta (ζ) potential that can be measured from electrokinetic measurements (Scheme 1).[18, 44, 55] At the salt concentrations explored here (50 mM NaCl), the ζ potential is distinct from the potential directly at the silica surface owing to the screening effect of ions within the Stern layer, which attenuate the magnitude of the potential at the OHP relative to that at the surface (Scheme 1). Moreover, calculations by the Netz group indicate that streaming current or streaming potential measurements (used to measure the zeta potential) are only sensitive to the Coulombic contributions from surface charges and screening by cations.[9] As we will discuss later on, this sensitivity of the ζ potential to only Coulombic contributions is not true of the total interfacial potential, which includes dipolar and higher-order contributions. $\chi^{(3)}$ is the third-order susceptibility of water in the diffuse layer which is frequency dependent[56] and has been shown by experiments and MD simulations to be relatively constant up to 100 mM ionic strength.[46, 56]

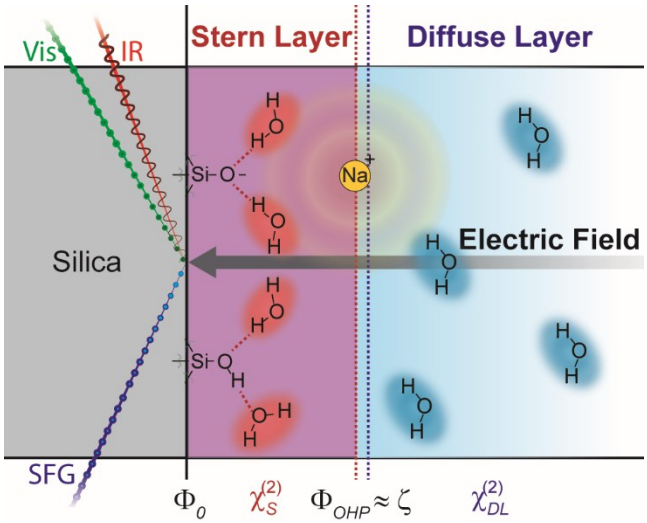

Scheme 1. The electrical double layer composed of a Stern layer (measured by $\chi_S^{(2)}$) and a diffuse layer (measured by $\chi_{DL}^{(2)}$) over negatively charged silica separated by the OHP (red dashed line). The net orientation and polarization of the diffuse layer is highlighted by the orientation of the drawn water structures, but we note a wide distribution is predicted for the diffuse layer water with its bulk-like structure.

Non-monotonic vs monotonic trends in SFG vs ζ-potential responses. Fig. 1a shows the (homodyne-detected) vibrational sum frequency generation intensity spectra of the fused silica/water interface in the presence of 50 mM NaCl from pH 10 to 2 measured in the OH stretching region. We chose this particular direction in our pH titration to stay close to the conditions reported in the XPS study of Stern layer thickness by Brown and co-workers.[44] Generally, three prominent features are observed that we refer to as the 3200, 3400, and 3600 cm^{-1} modes. These features arise from ordered and polarized interfacial water in the electrical double layer as described above,[34] although there is debate whether the 3600 cm^{-1} mode originates from isolated silanols[57-58] or water molecules dangling over hydrophobic silica sites.[59-60] At pH 10, the integrated SF intensity, which approximates the amount of net ordered and polarized water in the entire electrical double layer, is the largest (Fig. 1b). As the pH is lowered, the total SFG intensity decreases until pH 4 and then increases again slightly until pH 2, which lies near the point-of-zero charge (PZC) for silica, generally taken to be below pH 3, if any.[61] The origin of this non-monotonic trend, which we had observed previously at 100 mM and higher salt concentration,[62-64] is attributed to contributions to the nonlinear responses from the Stern and diffuse layers. Since these two components are convoluted in the SFG intensity measurements,[65] and further entangled with the electrostatic field across the interface, the exact origin of the non-monotonic trend is not yet clear.

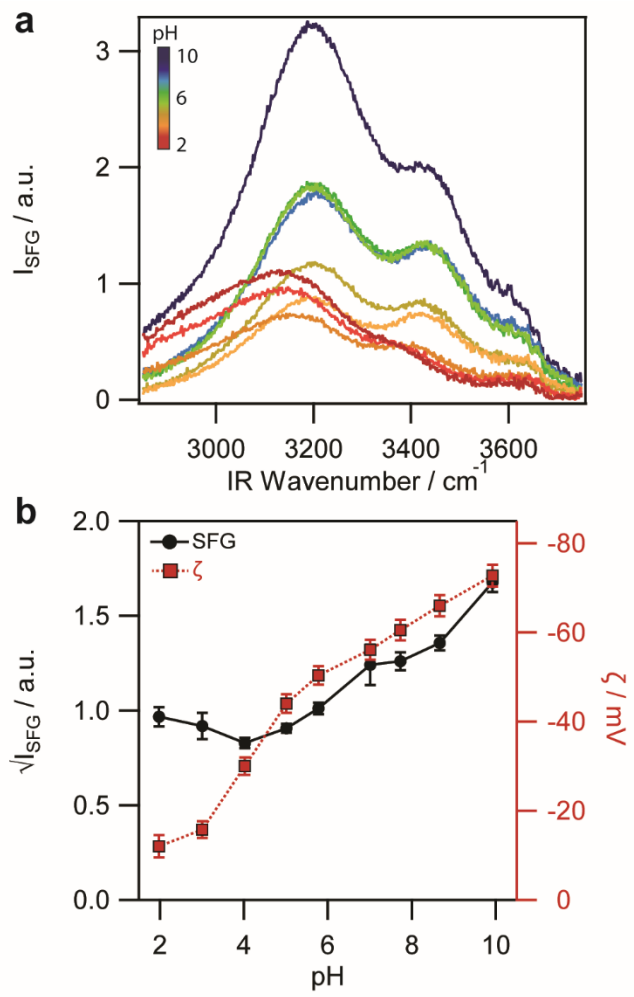

Figure 1. a) Vibrational sum frequency generation intensity spectra corrected for local field effects, (b) average square root of the integrated SFG intensities (left axis, black circles) from 2850-3750 cm^{-1}, and ζ potentials (right axis, red squares) determined by streaming potential measurements of the silica/aqueous interface in the presence of 50 mM NaCl from pH 10 to 2.

We can, however, estimate the behaviour of the diffuse layer contribution to the SF intensity if 1) the total OHP potential is known and 2) if the $\chi^{(3)}$ spectrum for the diffuse layer waters in the silica/water interface is known for our experimental conditions. The former can be approximated by measuring the ζ potential, while the latter is known from the literature.[46, 54, 56] Fig. 1b shows that our observed ζ potentials decreased monotonically in magnitude from high to low pH, consistent with an isoelectric point below pH 2 for this type of silica and salt

concentration.[61] Therefore, the diffuse layer contribution should only decrease with decreasing pH as $\chi^{(3)}$ is invariant with pH[56] and $\chi_{DL}^{(2)}$ is thereby only modulated by the Φ_{OHP}. With this insight it is clear that the Stern layer $\chi_S^{(2)}$ is playing a large role in the non-monotonic SF intensity changes observed below pH 4.

The Stern layer contribution, $\chi_S^{(2)}$, can be obtained by subtracting the diffuse layer contribution, $\chi_{DL}^{(2)}$, from the total nonlinear susceptibility, $\chi_{total}^{(2)}$. To determine the complex $\chi_{total}^{(2)}$ spectra, we require the phase, φ, of the SFG signal where $\left|\chi_{total}^{(2)}\right|e^{i\varphi} = Re\chi_{total}^{(2)} + iIm\chi_{total}^{(2)}$, which can be estimated using the maximum entropy method.[54, 66-75] However, the maximum entropy method phase (φ_{MEM}) is not the true phase of the SFG signal, φ. The difference between the two is called the error phase ($\varphi - \varphi_{MEM}$ = error phase). Determining the error phase is the main challenge of using the maximum entropy method to predict complex spectra as it must come from some external knowledge of the system.[76] Our previous work suggested that the error phase depended on the Debye length (i.e. the ionic strength), as the Debye length describes the depth of the diffuse layer (~4 κ^{-1}) and thus determines the phase matching condition for interference between the SFG signals generated throughout the various regions within the electrical double layer and the zero plane. The resulting phase shift is not captured by the MEM phase and, accordingly, must manifest as a shift in the error phase.[54]

Phase Relation between the Stern Layer $\chi_S^{(2)}$ and the $\chi^{(3)} \cdot \Phi(z)$ Product in the Diffuse Layer. In our present work, the salt concentration, and accordingly the Debye length, is maintained constant, so we would not expect a change in error phase. Surprisingly however, we observed a significant error phase change (~70° at 3300 cm^{-1}) when we analyzed the $\left|\chi_{total}^{(2)}\right|^2$ spectra and $\chi_{total}^{(2)}$ specta from Myalitsin et al.[77] at pH 7 and pH 2 at 10 mM ionic strength using the MEM

(Fig. S2). Using their[77] complex spectrum at pH 2 and our[54] complex spectrum at pH 6 as references, the error phases of our spectra herein were observed to decrease by ~100° (at 3300 cm^{-1}) from pH 6 to 2 (Fig. 2a). To understand this unexpected outcome, we turned to another nonlinear optical technique that has been used to measure phase changes at the silica/water interface, namely nonresonant heterodyne-detected second harmonic generation (HD-SHG) spectroscopy.[78-81] As we demonstrated recently, the phase shift measured by HD-SHG is related to the total sum frequency phase shift under conditions where the Debye length is changing,[54] suggesting their origins are related.

We therefore measured the SHG phase, φ_{sig}, between pH 10 and 2 at 50 mM NaCl by recording SHG intensity interferograms (Fig. 2b) from the fused silica/water interface as described in our earlier work (see SI Section S2).[78-81] Here, we report the relative phase, $\Delta\varphi_{sig}$, referenced to pH 5.8 and 50 mM NaCl and find that a phase shift in HD-SHG does indeed occur over the pH range (Fig. 2a and 2b). Fig. 2a also compares the relative phase change observed by HD-SHG and the change in error phase determined from our MEM analysis of the two reported complex spectra at pH 2 and 6. The HD-SHG phase shift is approximately two to three times smaller than the SF phase shift predicted at 3300 cm^{-1} using the MEM analysis. We hypothesize that this difference, which we did not observe when changing ionic strength,[54] is attributable to the differences between resonant SFG and nonresonant SHG relative signal magnitudes and phases of contributing oscillators (i.e. the $\chi_S^{(2)}/\chi_{DL}^{(2)}$ ratio) as these should impact the resulting total phase of the signal. Moreover, the nonresonant SHG signal contains contributions from all polarizable species including interfacial silanol groups, water, the ions, and protonated and deprotonated surface sites, whereas our vibrational SFG measurements only probe OH oscillators.[51, 64, 81] Finally, the SFG intensity spectra are subject to absorptive-dispersive mixing,[52-53, 82] which is not the case in the

non-resonant HD-SHG data. Nevertheless, the HD-SHG measurements allow us to predict how the error phase changes between our two reference points (i.e. pH 6 and pH 2) (Fig. 2a, blue line).

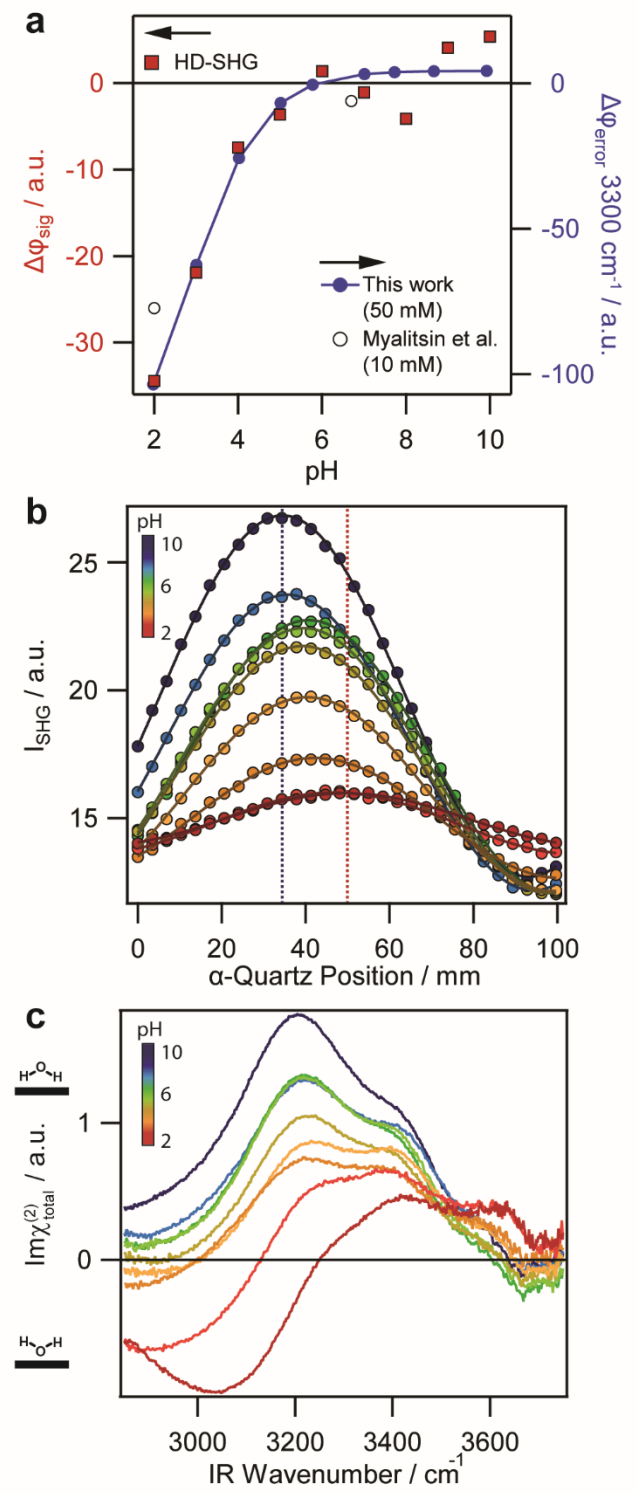

Figure 2. a) HD-SHG amplitudes and phases (red squares, left axis), and predicted error phase changes (blue dashed line, right axis) at the silica/water interface in the presence of 50 mM NaCl from pH 10 to 2. Error phase changes determined from reported HD-SFG measurements of the silica/10 mM sodium phosphate interface are shown as open circles (right axis).[77] Changes in HD-SHG and error phases (at 3300 cm^{-1}) are relative to their values at pH 5.8. b) Representative HD-SHG interferograms where solid lines are the cosine fits to the data (circles) and the blue and red dashed vertical lines indicate local maxima at pH 10 and 2, respectively. c) Imaginary $\chi^{(2)}_{total}$ spectra at the silica/50 mM NaCl interface determined using the maximum entropy method with reference to reported HD-SFG measurements.[54, 77]

With the error and SHG phases at each pH in hand, we performed the maximum entropy analysis of the spectra in Fig. 1a to yield $\left|\chi^{(2)}_{total}\right|e^{i\varphi_{MEM}}$ that was used to find the total complex spectra, $\left|\chi^{(2)}_{total}\right|e^{i\varphi} = Re\chi^{(2)}_{total} + iIm\chi^{(2)}_{total}$ from pH 10 to 2. The imaginary components of the spectra, $Im\chi^{(2)}_{total}$, report on the net orientation of the entire electrical double layer (Stern + diffuse layer) and are provided in Fig. 2c. At pH 10, $Im\chi^{(2)}_{total}$ is positive over the entire OH stretching region, indicating the net orientation of the water molecules that contribute in the EDL is with the hydrogen atoms pointed towards the silica.[54] As the pH is lowered, the 3200 and 3400 cm^{-1} modes decrease in magnitude while the 3600 cm^{-1} mode grows larger. Additionally, a broad negative feature around 3000 cm^{-1} appears and increases in magnitude as pH decreases. These general trends are consistent with the complex spectra measured by Myalitsin et al. at the silica/water interface and pH 2.1, 7.2, and 12.1[77] and also by Ostroverkhov et al. at the α-quartz/water interface,[83] which had been carried out over a similar pH range but at unspecified (and thus uncontrolled) ionic strengths. We emphasize that neither of these prior studies went beyond the reporting of $Im\chi^{(2)}_{total}$, i.e. they did not disentangle the Stern and diffuse layer contributions that are encoded in $\chi^{(2)}_{S}$ and the $\chi^{(3)} \cdot \Phi(z)$ product, respectively.

The change in sign of $Im\chi^{(2)}_{total}$ with decreasing pH is attributed to a net flip in the orientation of water molecules held in a strong hydrogen-bonding network.[84-85] According to eqn. 1 and 2, $Im\chi^{(2)}_{total}$ reports predominantly on Stern layer water molecules at pH 2, where the electrical potential is presumably small (and probably different from zero). However, at higher pH values, where the OHP potential, and hence the contribution from diffuse layer water molecules, is large, it is unclear how the Stern layer water molecules behave.

How Water Dipole Populations in the Stern and Diffuse Layer Vary with pH. To retrieve the Stern layer response, $\chi^{(2)}_S$, at all pH values, we multiply our previously determined $\chi^{(3)}$ spectrum for this interface and experimental geometry[54] by the OHP potentials we obtained from the streaming potential measurements and then subtract the resulting $\chi^{(3)} \cdot \Phi(z)$, i.e. $Im\chi^{(2)}_{DL}$, from $Im\chi^{(2)}_{total}$. The resulting pH-dependent $Im\chi^{(2)}_S$ and $Im\chi^{(2)}_{DL}$ spectra are shown in Fig. 3a and 3b, respectively. Within the Stern layer response, $\chi^{(2)}_S$, there may be a unique surface potential-dependent term arising from Stern layer water molecules that are oriented by the electric field near the surface (i.e. $\chi^{(3)}_{SL}\Phi_0$). Such an electric field-induced reorientation of interfacial water molecules is believed to be weaker than the existing H-bond network, based on MD simulations[86] and calculations.[54] Yet, we do not know the Stern layer third-order susceptibility, $\chi^{(3)}_{SL}$, which should exhibit a different line-shape than the diffuse layer third-order susceptibility, $\chi^{(3)}$, owing to differences in hydrogen bond structure. Consequently, we do not attempt to deconvolute any surface-potential dependence from the Stern layer spectra we present. Fig. 3a shows the dominant pH dependence occurs in the low frequency region, indicating changes in pH caused changes in the orientation of water molecules located in the strongly hydrogen-bonded network in the Stern layer. This result is consistent with a purely mathematical lineshape analysis of vibrational SFG

model responses at charged aqueous interfaces, which showed the highest sensitivity in the 3200 cm^{-1} region.[53]

As mentioned earlier, the sign of $Im\chi_S^{(2)}$ reports on waters oscillators with dipoles pointing towards the silica (positively signed modes) or towards the bulk aqueous phase (negatively signed modes). At pH 10, $Im\chi_S^{(2)}$ contains a large positive feature centred around 3150 cm^{-1}, a shallow negative feature around 3400 cm^{-1}, and a narrower positive feature at 3600 cm^{-1} (Fig. 3a). As the pH is lowered the large broad positively signed mode at low wavenumber decreases in magnitude while a similarly broad negative mode grows in at slightly redshifted frequencies. Conversely, the shallow feature around 3400 cm^{-1} flips in sign as the pH is decreased. Near the point-of-zero-charge around pH 2, a large negatively signed feature around 3050 cm^{-1} is observed. Based on its sign, this mode can be assigned to water molecules that accept H-bonds from the surface while the smaller positively signed feature around 3400 cm^{-1} can be assigned to water molecules which donate H-bonds to silica.[49, 77] We also note that the net orientation of the water molecules in the tighter (<3300 cm^{-1}) vs looser (3300 cm^{-1} to 3500 cm^{-1}) hydrogen bond network tends to be opposite from one another at any given pH, and that their pH dependence is also counter to one another.

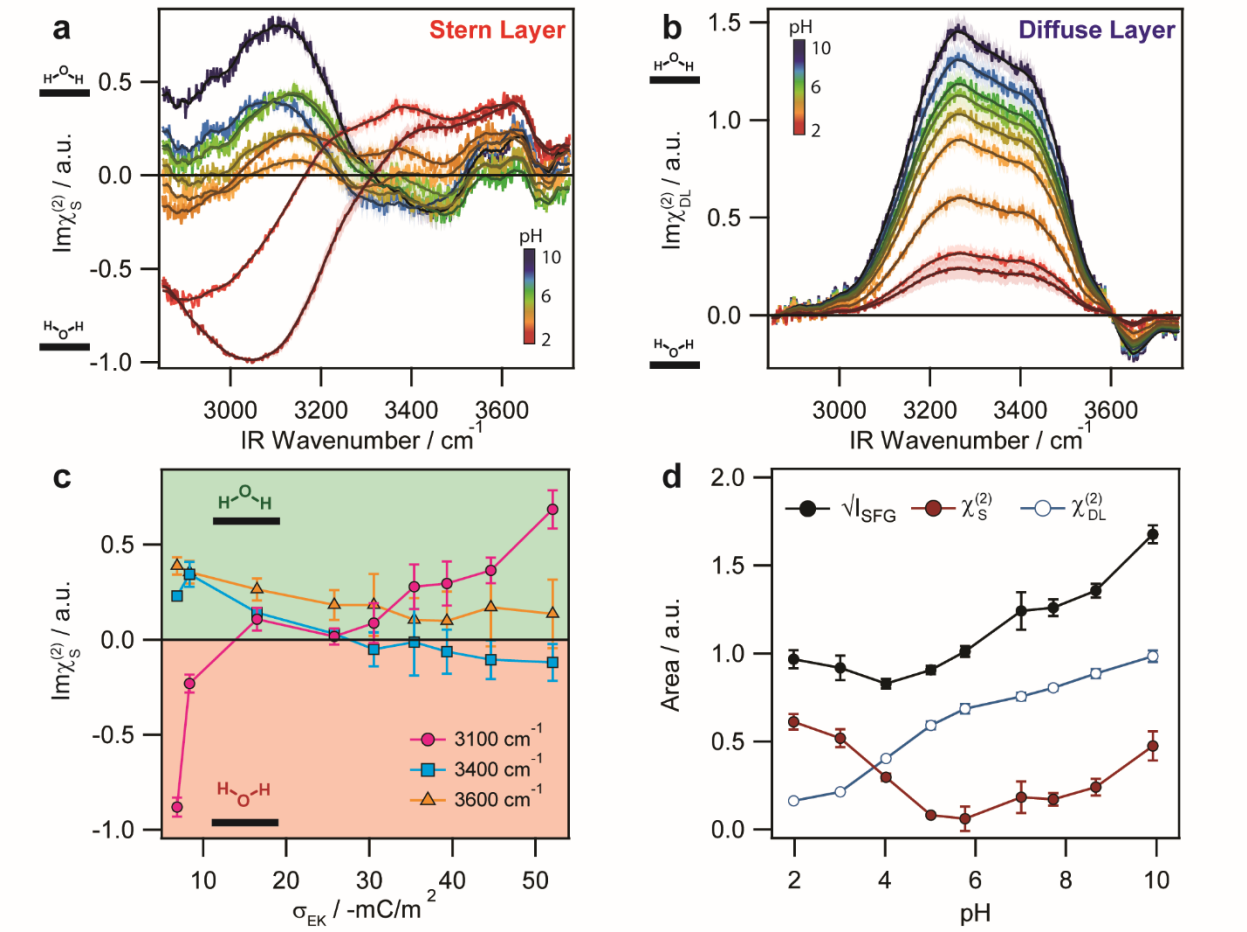

Figure 3. Contributions to the total imaginary complex spectra, $Im\chi_{total}^{(2)}$, of the silica/water interface in the presence of 50 mM NaCl from pH 10 to 2 originating from a) the Stern layer and b) the diffuse layer. c) $Im\chi_S^{(2)}$ amplitudes at 3100, 3400, and 3600 cm^{-1} with respect to electrokinetic charge densities calculated from the ζ potentials. d) Average square root of the integrated SFG intensities (black squares), the Stern layer (red closed circles), and the diffuse layer (blue open circles) contributions to the total complex spectra, $\chi_{total}^{(2)}$.

Each surface silanol group can, in principle, coordinate two H-bond donor water molecules and one H-bond acceptor water, but the 3400 cm^{-1} mode attributed to the former is smaller than the 3050 cm^{-1} mode, possibly due to partial cancellation of signal contributions from some oppositely oriented H-bond donors.[49, 64] The decrease in magnitude of both the negatively signed 3050 cm^{-1} mode and the positively signed 3400 cm^{-1} mode with increasing pH is consistent with silanol deprotonation (Fig. 3c, charge densities from our pH-dependent ζ potential measurements).

Concurrently, the increase in magnitude of the positively signed mode around 3150 cm^{-1} with increasing pH is consistent with an increasing number of water molecules which donate H-bonds to siloxide sites.[54, 87] However, the steep magnitude decrease at 3100 cm^{-1} with an increase in surface charge density is noteworthy as it reveals that the number of hydrogen-bond accepting water molecules quickly reduces as the surface is deprotonated despite the substantial amount of silanol sites that should remain even at the highest pH (80% of sites at pH 10 are still neutral SiOH groups, according to XPS data).[43] Fig. 3c then suggests that the number of water molecules contributing to each population of the two types of hydrogen bond networks within the Stern layer is influenced not only by the number of sites but also interactions between the oriented water molecules and the electric field and charges within the Stern layer, which is in agreement with a very recent report on silica particles.[88] At higher pH, this electric field should become increasingly repulsive to the dipole moment of water molecules oriented as hydrogen-bond acceptors with surface sites.

The positively signed 3600 cm^{-1} peak, which was observed in the intensity spectra and previously assigned to either isolated silanol groups[57-58] or dangling water molecules over hydrophobic sites,[59-60] is present in the Stern layer spectra and remains positively signed over the entire titration (Fig. 3c). Its pH-invariant sign is consistent with the notion that this mode originates from OH oscillators that are directed with their hydrogen pointed away from the water and into the silica. These are presumably SiOH groups located in water-inaccessible sub-nanosized pockets that are part of the $\chi^{(2)}$-active interfacial region. Our recently published AFM scans of the fused silica used in the HD-SHG experiments (Hyperion) show an rms-roughness of 0.4 nm with height variations of up to 1 nm,[81] which would be consistent with this interpretation.

The origin of the negatively signed 3400 cm^{-1} feature at high pH is unclear, however it may arise from uncoupled H-bond donor water molecules near SiO^- groups; at 2 M NaCl and pH 12, Urashima et al. determined the OH oscillators contributing to their HD-SFG spectra in this range were completely uncoupled owing to the similarity between the silica/H_2O and silica/HOD interfaces.[87] In those spectra, a small negatively signed feature around 3500 cm^{-1} was also observed, which was assigned to the uncoupled OH oscillator of the aforementioned H-bond donor water directed into the bulk water.

Our analysis reveals that the OH oscillators in the Stern layer flip their orientation as the pH changes from pH 10 to 2, except for those resonating at 3600 cm^{-1}. This trend is not apparent from the intensity spectra or even the $Im\chi^{(2)}_{total}$ spectra. Integrating the $\chi^{(2)}_S$ spectra over the entire frequency range studied (Fig. 3d) reveals the non-monotonic trend observed in the SFG intensity spectra (Fig. 1), with a minimum occurring at pH 6. The greatest amount of ordered and net-polarized water molecules in the Stern layer occurs near the PZC at pH 2. Furthermore, at pH 2 the H-bond network is apparently stronger than at higher pH, which is evident from the relatively redshifted frequencies. In contrast, the integrated diffuse layer spectra only increase in magnitude as the pH is increased. We conclude that the non-monotonic trend observed in the SFG intensity spectra originates entirely from the water molecules located within the tight and loose hydrogen bond networks of the Stern layer.

Connecting Stern Layer Structure with Coulomb, Dipole, and Other Contributions to Φ_{tot}. Finally, we analyze the pH-dependent HD-SHG measurements from Fig. 2b to yield an interfacial potential value for each pH. In contrast to the ζ potential, this HD-SHG measurement yields the total interfacial potential drop across the solid/liquid interface and is the sum of Coulombic, dipolar, quadrupolar, and other contributions to the total electrostatic potential difference between the bulk

silica and the aqueous bulk.[81] Our earlier pH titration at 0.5 M NaCl showed this potential to map 1:1 onto potential estimates from impedance measurements of oxide-terminated FETs.[89-90]

In the 50 mM pH titration analyzed here, the HD-SHG-determined (i.e. total surface) potential becomes neutral near pH 3 and positive at lower pH (+17 mV ± 10% at pH 2, Fig. 4d).[81] In contrast, our streaming potential measurements (Fig. 1b) indicate that the ζ potential remains negative over the entire pH range (pH 10 to pH 2, 50 mM ionic strength, Fig. 1b). Oppositely signed surface potentials (measured by an ion-sensitive FET device, which also provides the total surface potential) and ζ potentials have also been observed near the point-of-zero-charge of a single crystal quartz electrode in 10 mM NaCl.[23] We provide two explanations for the opposite signs between the ζ potentials (arising at the outer Helmholtz plane) and the total surface potential (arising at the 0-plane). The first explanation stems from the observed flip in net orientation of the tightly H-bonded water molecules in the Stern layer (contributing at 3100 cm^{-1}) at ~ pH 4 as the pH decreases from pH 10 to 2 (Fig. 3a). It has been argued that like in FET- and X-ray- based measurements of the surface potential, the total potential that is probed by HD-SHG includes not only the Coulombic contribution from ions but also dipole contributions from the ordered water molecules (the water dipole potential),[81] while, as mentioned earlier, electrokinetic measurements of the ζ potential are only sensitive to the Coulombic contributions, according to Netz and co-workers.[9] In addition to surface charges, these water dipoles have been known to play a key role in the electrical and structural properties of the EDL over electrochemical interfaces in the form of the "δχ potential" (no relation to $\chi^{(2)}$ or $\chi^{(3)}$).[91-92]

We now propose that the relative magnitude and sign (i.e. direction) of the dipole potential from ordered water in the Stern layer can be estimated from the $Im\chi_S^{(2)}$ (surface) spectra as it reports the extent of order and net direction of the dipolar array of water molecules in the Stern

layer. At pH 10, the Stern layer is highly ordered with the net orientation of water molecules pointing their hydrogen atoms towards the surface. This general orientation is the same in the diffuse layer at this pH as both the Stern and diffuse layer spectra are dominated by positive features. A qualitative estimate for the corresponding potentials arising from the aligned dipole moments in each layer is shown in Fig. 4a. As our HD-SHG analysis provides the sum of all of these potentials, it should be substantially more negative than the ζ potential at pH 10, which is indeed observed (-410 mV vs -73 mV, respectively)[81]. This difference in potential is consistent with the large dipole potentials on the order of hundreds of millivolts measured at the neat water/air interface using ionizing surface potential methods.[11] However at pH 2, the case is different. At this low pH, the Stern layer is also well ordered with the water molecules net-oriented with their oxygen atoms pointed towards the surface (negative features in $Im\chi_S^{(2)}$), while the water molecules in the diffuse layer are oriented in the opposite direction owing to the negative ζ potential. The resulting dipole potential should be much larger in the Stern layer and opposite in sign to that in the diffuse layer (because the diffuse layer spectrum is smaller in magnitude to that of the Stern layer at pH 2). If the surface is still slightly negative at pH 2 (i.e. more SiO^- than $SiOH_2^+$ sites) then the Coulombic potential at the surface would still be negative and slightly larger in magnitude to the ζ potential from the outer Helmholtz plane. Based on this scenario, the HD-SHG-determined potential could be positive at pH 2 because the significant contribution of the water dipole potential from the Stern layer overwhelms the oppositely charged surface Coulombic potential (Fig. 4b), while the ζ potential stemming from the Coulombic potential at the outer Helmholtz plane is still negative.

The second scenario is a simpler explanation for the different signed potentials from SHG and streaming potential measurements. If the silica surface (0-plane) is indeed net positively

charged at pH 2, then one possible reason for the negative ζ potential is the enhancement of chloride ions in the Stern layer (more chloride ions near the surface than positively charged sites) leading to a more negative potential at the OHP than at the surface (Fig. 4c). Future work will explore the impact of different counter-ions particularly near the point-of-zero charge to help distinguish between the two proposed mechanisms.

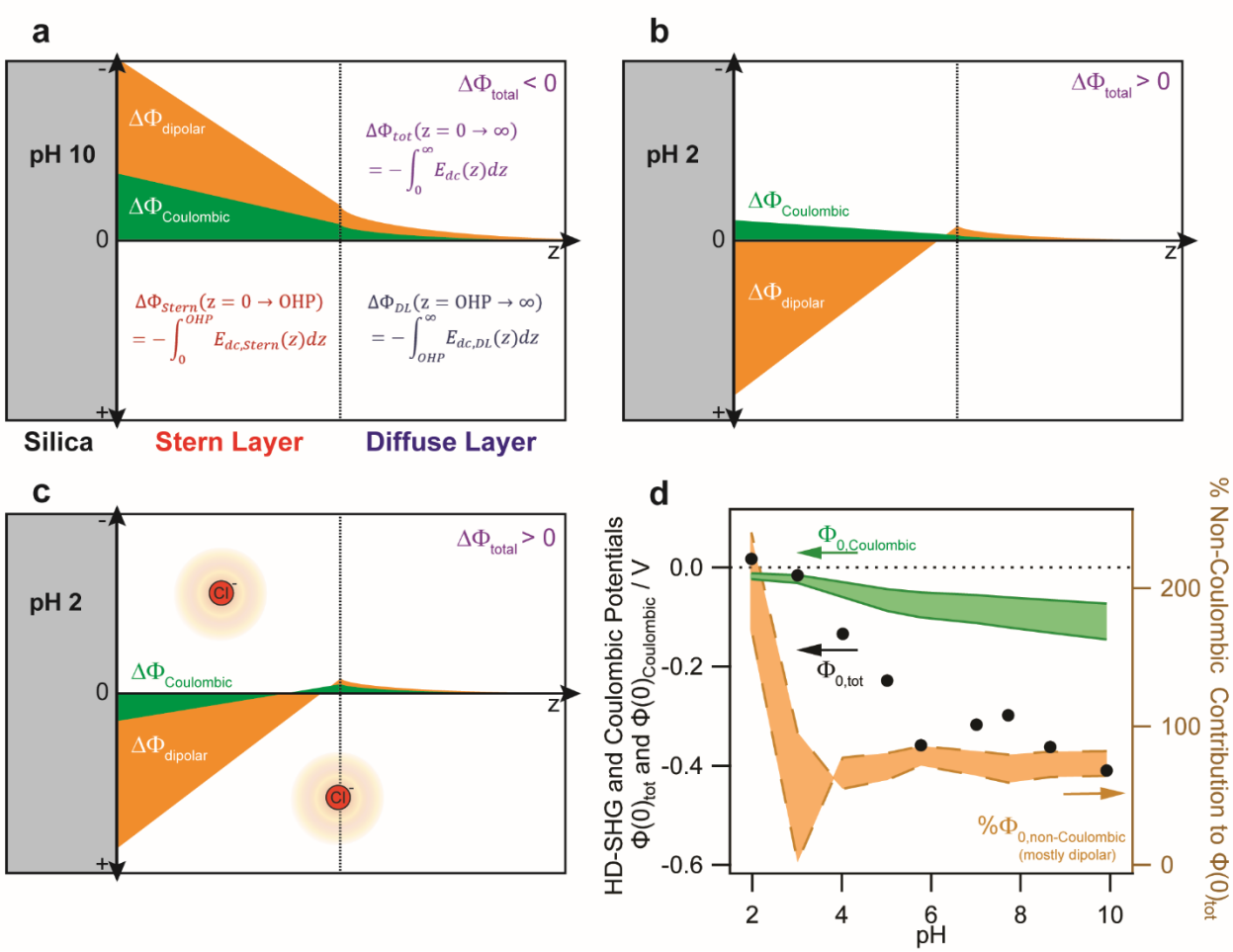

Figure 4. Coulombic (green) and water dipole (gold, behind green) potential contributions to the total electric potential, which is the sum of the green and gold curves, at the silica/water interface at a) pH 10, b) pH 2 in the case of a negatively charged surface and c) pH 2 in the case of chloride enhancement within the Stern layer due to a positively charged surface. The chloride ions of c) represent an excess of negative charges near a positive surface resulting in charge inversion and a negative potential at the OHP. The Coulombic potential arises from the static electric field emanating from charges at the surface while the water dipole potential arises from the sum of water dipole electric fields. In cases b) and c) the total electric potential would appear the same despite the different mechanisms. The differences in potential magnitudes between high and low pH and

between Coulombic and dipolar contributions are qualitative for clarity. d) The HD-SHG-determined potentials of the silica/water interface at 50 mM NaCl ($\Phi_{0,tot}$, black circles, left axis), the total Coulombic (Gouy-Chapman) potentials ($\Phi_{0,Coulombic}$, green shaded region, left axis) estimated as one to two times the ζ potential under scenario b), and the percent to the total potential arising from non-Coulombic contributions (gold shaded region, right axis).

Conclusions

In summary, we separated the vibrational sum frequency signal from the silica/water interface into Stern and diffuse layer contributions using the maximum entropy method, complementary heterodyne-detected second harmonic generation, and streaming potential measurements while appropriately accounting for phase matching and absorptive-dispersive mixing. The integrated SFG intensities reporting on the total amount of ordered water in the EDL exhibit a non-monotonic trend with a minimum at pH 4. Yet, ζ potential measurements at the same interface only decrease in magnitude with decreasing pH. Since the ζ potentials are responsible for aligning the diffuse layer water molecules, the non-monotonic trend observed by SFG was identified to originate from the interplay of Stern layer water molecules in tight and loosely H-bonded networks. The maximum entropy method was used with error phases determined from previous phase-sensitive SFG and complementary heterodyned SHG experiments to retrieve the complex SFG spectra from the measured intensities, for which the imaginary component reports on the absolute molecular orientation for the various Stern layer water dipole populations. The Stern layer spectra were then obtained by coupling our recently determined $\chi^{(3)}$ spectrum[54] to the measured ζ potentials and subtracting the resulting diffuse layer spectra from the total complex spectra derived from the maximum entropy method.

The imaginary parts of the Stern layer spectra exhibit a flip in sign upon decreasing the pH from 10 to pH 2, particularly for water molecules in the tight H-bond network (stretching frequencies <3300 cm^{-1}). The minimum in structural order occurs at pH 6 at this salt concentration

of 50 mM, which suggests that at this pH the surface is deprotonated enough to generate a surface electric field that disrupts neutral silanol sites from interacting with hydrogen bond acceptors. However, the low density of siloxides at this pH does not allow for much interaction with water hydrogen-bond donors. At higher pH, the latter population begins to dominate at low wavenumber.

We also find through the total potential drop across the fused silica/electrolyte interface provided by our HD-SHG experiments that the Coulomb-only contribution provided by the widely used Gouy-Chapman or Gouy-Chapman-Stern model vastly underestimates the interfacial electrostatics. Indeed, over three quarters of the total potential are due to non-Coulombic contributions, presumably the dipolar, quadrupolar, and higher-order contributions. These contributions are not sampled in electrokinetic measurements of ζ or streaming potentials, as was recently shown by Netz and co-workers,[9] and we provide an estimate from our experimental data here for the various pH values investigated. Our findings also underscore the importance of properly accounting for the $\chi^{(3)}$ contribution in the analysis of the vibrational lineshapes provided by second-order spectroscopic studies of charged aqueous interfaces. To this end, the interfacial potential is needed. The method presented here, in which SFG and SHG spectroscopy are paired, is proposed as a clear path to take. Taken together, our results provide the first vibrational Stern layer spectra of the silica/water interface over a wide pH range at controlled ionic strength. Moreover, they indicate an important role of non-Coulombic contributions to the total potential drop across the oxide/water interface, accounting for greater than half and more, depending on pH. Our analysis may be applied to many charged surface/aqueous interfaces to spectrally separate the Stern and diffuse layers given the appropriate complex spectra are available for reference.

ASSOCIATED CONTENT

Supporting Information

The following files are available free of charge via the Internet at https://pubs.acs.org.

The supporting information contains: experimental details, calculations for local field effects in SFG spectra, in-depth details of error phase prediction using the MEM, and electrokinetic charge densities calculated from zeta potentials.

AUTHOR INFORMATION

Corresponding Author

*E-mail: julianne.gibbs@ualberta.ca (J.M.G.)

*E-mail: f-geiger@northwestern.edu (F.M.G.)

Notes

The authors declare no competing financial interest.

ACKNOWLEDGEMENTS

J.M.G. gratefully acknowledges the Natural Sciences and Engineering Research Council of Canada for an Accelerator Award, the Alfred P. Sloan Foundation for a Research Fellowship, and Petro-Canada for a Young Innovator Award. B.R. gratefully acknowledges support from the Alberta/Technical University of Munich International Graduate School for Hybrid Functional Materials (ATUMS-NSERC CREATE) program, the Natural Sciences and Engineering Research Council of Canada for a Canadian Graduate Scholarship, and the Queen Elizabeth II Graduate Scholarship. F.M.G. and E.M. gratefully acknowledge support from the AFOSR Molecular Dynamics and Theoretical Chemistry Program and from Northwestern University. We thank Dr. Hore (University of Victoria) for insightful discussions.

REFERENCES

1. Langmuir, D., *Aqueous Environmental Chemistry*. Prentice Hall: Upper Saddle River, NJ 1997.
2. Lyklema, J., *Fundamentals of Interface and Colloid Science*. Elsevier: 2000.
3. Helmholtz, H., Ueber Einige Gesetze der Vertheilung Elektrischer Ströme in Körperlichen Leitern mit Anwendung auf die Thierisch-Elektrischen Versuche. *Ann. Phys.-Berlin* **1853,** *165* (6), 211-233.

4. Gouy, M., Sur la Constitution de la Charge Électrique à la Surface d'un Électrolyte. *J. Phys. Theor. Appl.* **1910,** *9* (1), 457-468.
5. Chapman, D. L., LI. A Contribution to the Theory of Electrocapillarity. *Philos. Mag.* **1913,** *25* (148), 475-481.
6. Stern, O., Zur Theorie der Elektrolytischen Doppelschicht. *Z. Elktrochem. Angew. P.* **1924,** *30* (21-22), 508-516.
7. Grahame, D. C., The Electrical Double Layer and the Theory of Electrocapillarity. *Chem. Rev.* **1947,** *41* (3), 441-501.
8. Casper, C. B.; Verreault, D.; Adams, E. M.; Hua, W.; Allen, H. C., Surface Potential of DPPC Monolayers on Concentrated Aqueous Salt Solutions. *J. Phys. Chem. B* **2016,** *120* (8), 2043-2052.
9. Bonthuis, D. J.; Horinek, D.; Bocquet, L.; Netz, R. R., Electrohydraulic Power Conversion in Planar Nanochannels. *Phys. Rev. Lett.* **2009,** *103* (14), 144503.
10. Rodriguez, D.; Marquez, M. D.; Zenasni, O.; Han, L. T.; Baldelli, S.; Lee, R. T., Surface Dipoles Induce Uniform Orientation in Contacting Polar Liquids. *Chem. Mat.* **2020,** *32*, 7832-41.
11. Adel, T.; Velez-Alvarez, J.; Co, A. C.; Allen, H. C., Circuit Analysis of Ionizing Surface Potential Measurements of Electrolyte Solutions. *J. Electrochem. Soc.* **2021,** *168* (1), 016507.
12. Doyle, C. C.; Shi, Y.; Beck, T. L., The Importance of the Water Molecular Quadrupole for Estimating Interfacial Potential Shifts Acting on Ions Near the Liquid−Vapor Interface. *J. Phys. Chem. B* **2019,** *123*, 3348-58.
13. Cendagorta, J. R.; Ichiye, T., The Surface Potential of the Water-Vapor Interface from Classical Simulations. *J. Phys. Chem. B* **2015,** *119*, 9114-9122.
14. Leung, K., Surface Potential at the Air-Water Interface Computed Using Density Functional Theory. *J. Phys. Chem. Lett.* **2010,** *1*, 496-9.
15. Ma, E.; Kim, J.; Chang, H.; Ohno, P. E.; Jodts, R. J.; Miller III, T. F.; Geiger, F. M., Stern and Diffuse Layer Interactions during Ionic Strength Cycling. *J. Phys. Chem. C* **2021,** *125*, 18002-14.
16. Chen, S.-H.; Singer, S., Molecular Dynamics Study of the Electric Double Layer and Nonlinear Spectroscopy at the Amorphous Silica- Water Interface. *J. Phys. Chem. A* **2019,** *123*, 6364-84.
17. Dewan, S.; Carnevale, V.; Bankura, A.; Eftekhari-Bafrooei, A.; Fiorin, G.; Klein, M. L.; Borguet, E., Structure of Water at Charged Interfaces: A Molecular Dynamics Study. *Langmuir* **2014,** *30*, 8056-65.
18. Brown, M. A.; Abbas, Z.; Kleibert, A.; Green, R. G.; Goel, A.; May, S.; Squires, T. M., Determination of Surface Potential and Electrical Double-Layer Structure at the Aqueous Electrolyte-Nanoparticle Interface. *Phys. Rev. X* **2016,** *6* (1), 011007.
19. Mayordomo, N.; Foerstendorf, H.; Lützenkirchen, J.; Heim, K.; Weiss, S.; Alonso, U.; Missana, T.; Schmeide, K.; Jordan, N., Selenium(IV) Sorption Onto γ-Al2O3: A Consistent Description of the Surface Speciation by Spectroscopy and Thermodynamic Modeling. *Environ. Sci. Technol.* **2018,** *52* (2), 581-588.
20. Öhman, L. O.; Lövgren, L.; Hedlund, T.; Sjöberg, S., Chapter 1 - The Ionic Strength Dependency of Mineral Solubility and Chemical Speciation in Solution. In *Interface Science and Technology*, Lützenkirchen, J., Ed. Elsevier: 2006; Vol. 11, pp 1-34.
21. Kosmulski, M., Co-Adsorption of Mono- and Multivalent Ions on Silica and Alumina. *Ber. Bunsenges. Phys. Chem* **1994,** *98* (8), 1062-1067.
22. Fung, C. D.; Cheung, P. W.; Ko, W. H., A Generalized Theory of an Electrolyte-Insulator-Semiconductor Field-Effect Transistor. *IEEE T. Electron. Dev.* **1986,** *33* (1), 8-18.
23. Preočanin, T.; Namjesnik, D.; Brown, M. A.; Lützenkirchen, J., The Relationship Between Inner Surface Potential and Electrokinetic Potential from an Experimental and Theoretical Point of View. *Environ. Chem.* **2017,** *14* (5), 295-309.
24. Raji, F.; Ejtemaei, M.; Nguyen, A. V., Resolving the Mystery of the Second Charge Reversal on Solid Surfaces in the Presence of Divalent Heavy Metal Ions. *Appl. Surf. Sci.* **2020,** *529*, 147128.

25. de Lint, W. B. S.; Benes, N. E.; Lyklema, J.; Bouwmeester, H. J. M.; van der Linde, A. J.; Wessling, M., Ion Adsorption Parameters Determined from Zeta Potential and Titration Data for a γ-Alumina Nanofiltration Membrane. *Langmuir* **2003,** *19* (14), 5861-5868.
26. Zhang, Z.; Fenter, P.; Cheng, L.; Sturchio, N. C.; Bedzyk, M. J.; Předota, M.; Bandura, A.; Kubicki, J. D.; Lvov, S. N.; Cummings, P. T.; Chialvo, A. A.; Ridley, M. K.; Bénézeth, P.; Anovitz, L.; Palmer, D. A.; Machesky, M. L.; Wesolowski, D. J., Ion Adsorption at the Rutile−Water Interface: Linking Molecular and Macroscopic Properties. *Langmuir* **2004,** *20* (12), 4954-4969.
27. Sverjensky, D. A., Prediction of the Speciation of Alkaline Earths Adsorbed on Mineral Surfaces in Salt Solutions. *Geochim. Cosmochim. Ac.* **2006,** *70* (10), 2427-2453.
28. Morag, J.; Dishon, M.; Sivan, U., The Governing Role of Surface Hydration in Ion Specific Adsorption to Silica: An AFM-Based Account of the Hofmeister Universality and Its Reversal. *Langmuir* **2013,** *29* (21), 6317-6322.
29. van Lin, S. R.; Grotz, K. K.; Siretanu, I.; Schwierz, N.; Mugele, F., Ion-Specific and pH-Dependent Hydration of Mica–Electrolyte Interfaces. *Langmuir* **2019,** *35* (17), 5737-5745.
30. Brown Gordon, E., How Minerals React with Water. *Science* **2001,** *294* (5540), 67-69.
31. Lee, S. S.; Fenter, P.; Nagy, K. L.; Sturchio, N. C., Real-Time Observation of Cation Exchange Kinetics and Dynamics at the Muscovite-Water Interface. *Nat. Commun.* **2017,** *8* (1), 15826.
32. Geiger, F. M., Second Harmonic Generation, Sum Frequency Generation, and $\chi^{(3)}$: Dissecting Environmental Interfaces with a Nonlinear Optical Swiss Army Knife. *Annu. Rev. Phys. Chem.* **2009,** *60*, 61-83.
33. Covert, P. A.; Hore, D. K., Geochemical Insight from Nonlinear Optical Studies of Mineral–Water Interfaces. *Annu. Rev. Phys. Chem.* **2016,** *67* (1), 233-257.
34. Backus, E. H. G.; Schaefer, J.; Bonn, M., Probing the Mineral–Water Interface with Nonlinear Optical Spectroscopy. *Angew. Chem. Int. Ed.* **2021,** *60* (19), 10482-10501.
35. Nakouzi, E.; Stack, A. G.; Kerisit, S.; Legg, B. A.; Mundy, C. J.; Schenter, G. K.; Chun, J.; De Yoreo, J. J., Moving beyond the Solvent-Tip Approximation to Determine Site-Specific Variations of Interfacial Water Structure through 3D Force Microscopy. *J. Phys. Chem. C* **2021,** *125* (2), 1282-1291.
36. Harmon, K. J.; Chen, Y.; Bylaska, E. J.; Catalano, J. G.; Bedzyk, M. J.; Weare, J. H.; Fenter, P., Insights on the Alumina–Water Interface Structure by Direct Comparison of Density Functional Simulations with X-ray Reflectivity. *J. Phys. Chem. C* **2018,** *122* (47), 26934-26944.
37. Lee, S. S.; Schmidt, M.; Laanait, N.; Sturchio, N. C.; Fenter, P., Investigation of Structure, Adsorption Free Energy, and Overcharging Behavior of Trivalent Yttrium Adsorbed at the Muscovite (001)–Water Interface. *J. Phys. Chem. C* **2013,** *117* (45), 23738-23749.
38. Lee, S. S.; Park, C.; Sturchio, N. C.; Fenter, P., Nonclassical Behavior in Competitive Ion Adsorption at a Charged Solid–Water Interface. *J. Phys. Chem. Lett.* **2020,** *11* (10), 4029-4035.
39. Fenter, P.; Sturchio, N. C., Mineral–Water Interfacial Structures Revealed by Synchrotron X-Ray Scattering. *Prog. Surf. Sci.* **2004,** *77* (5), 171-258.
40. Park, C.; Fenter, P. A.; Nagy, K. L.; Sturchio, N. C., Hydration and Distribution of Ions at the Mica-Water Interface. *Phys. Rev. Lett.* **2006,** *97* (1), 016101.
41. Fenter, P.; Cheng, L.; Rihs, S.; Machesky, M.; Bedzyk, M. J.; Sturchio, N. C., Electrical Double-Layer Structure at the Rutile–Water Interface as Observed in Situ with Small-Period X-Ray Standing Waves. *J. Colloid Interf. Sci.* **2000,** *225* (1), 154-165.
42. Schlegel, M. L.; Nagy, K. L.; Fenter, P.; Sturchio, N. C., Structures of Quartz (100)- and (101)-Water Interfaces Determined by X-Ray Reflectivity and Atomic Force Microscopy of Natural Growth Surfaces. *Geochim. Cosmochim. Ac.* **2002,** *66* (17), 3037-3054.
43. Duval, Y.; Mielczarski, J. A.; Pokrovsky, O. S.; Mielczarski, E.; Ehrhardt, J. J., Evidence of the Existence of Three Types of Species at the Quartz−Aqueous Solution Interface at pH 0−10: XPS Surface Group Quantification and Surface Complexation Modeling. *J. Phys. Chem. B* **2002,** *106* (11), 2937-2945.

44. Brown, M. A.; Goel, A.; Abbas, Z., Effect of Electrolyte Concentration on the Stern Layer Thickness at a Charged Interface. *Angew. Chem. Int. Ed.* **2016,** *55*, 3790 - 3794.
45. Joutsuka, T.; Hirano, T.; Sprik, M.; Morita, A., Effects of Third-Order Susceptibility in Sum Frequency Generation Spectra: A Molecular Dynamics Study in Liquid Water. *Phys. Chem. Chem. Phys.* **2018,** *20* (5), 3040-3053.
46. Joutsuka, T.; Morita, A., Electrolyte and Temperature Effects on Third-Order Susceptibility in Sum-Frequency Generation Spectroscopy of Aqueous Salt Solutions. *J. Phys. Chem. C* **2018,** *122* (21), 11407-11413.
47. Pezzotti, S.; Galimberti, D. R.; Shen, Y. R.; Gaigeot, M.-P., Structural Definition of the BIL and DL: A New Universal methodology to Rationalize Non-Linear $\chi^{(2)}(\omega)$ SFG Signals at Charged Interfaces, Including $\chi^{(3)}(\omega)$ Contributions. *Phys. Chem. Chem. Phys.* **2018,** *20* (7), 5190-5199.
48. Pezzotti, S.; Galimberti, D. R.; Gaigeot, M.-P., Deconvolution of BIL-SFG and DL-SFG Spectroscopic Signals Reveals Order/Disorder of Water at the Elusive Aqueous Silica Interface. *Phys. Chem. Chem. Phys.* **2019,** *21* (40), 22188-22202.
49. Roy, S.; Hore, D. K., Simulated Structure and Nonlinear Vibrational Spectra of Water Next to Hydrophobic and Hydrophilic Solid Surfaces. *J. Phys. Chem. C* **2012,** *116* (43), 22867-22877.
50. Gonella, G.; Lütgebaucks, C.; de Beer, A. G. F.; Roke, S., Second Harmonic and Sum-Frequency Generation from Aqueous Interfaces Is Modulated by Interference. *J. Phys. Chem. C* **2016,** *120* (17), 9165-9173.
51. Wang, H.; Hu, X.-H.; Wang, H.-F., Charge-Induced χ(3) Susceptibility in Interfacial Nonlinear Optical Spectroscopy Beyond the Bulk Aqueous Contributions: The Case for Silica/Water Interface. *J. Phys. Chem. C* **2021,** *125* (47), 26208-26215.
52. Ohno, P. E.; Wang, H.-f.; Geiger, F. M., Second-Order Spectral Lineshapes from Charged Interfaces. *Nat. Commun.* **2017,** *8* (1), 1032.
53. Ohno, P. E.; Wang, H.-f.; Paesani, F.; Skinner, J. L.; Geiger, F. M., Second-Order Vibrational Lineshapes from the Air/Water Interface. *J. Phys. Chem. A* **2018,** *122* (18), 4457-4464.
54. Rehl, B.; Gibbs, J. M., Role of Ions on the Surface-Bound Water Structure at the Silica/Water Interface: Identifying the Spectral Signature of Stability. *J. Phys. Chem. Lett.* **2021,** *12* (11), 2854-2864.
55. Lyklema, J., *Solid-Liquid Interfaces*. Academic Press: San Diego, 1995; Vol. II.
56. Wen, Y.-C.; Zha, S.; Liu, X.; Yang, S.; Guo, P.; Shi, G.; Fang, H.; Shen, Y. R.; Tian, C., Unveiling Microscopic Structures of Charged Water Interfaces by Surface-Specific Vibrational Spectroscopy. *Phys. Rev. Lett.* **2016,** *116* (1), 016101.
57. Dalstein, L.; Potapova, E.; Tyrode, E., The Elusive Silica/Water Interface: Isolated Silanols Under Water as Revealed by Vibrational Sum Frequency Spectroscopy. *Phys. Chem. Chem. Phys.* **2017,** *19*, 10343-10349.
58. Rashwan, M.; Rehl, B.; Sthoer, A.; Darlington, A. M.; Azam, M. S.; Zeng, H.; Liu, Q.; Tyrode, E.; Gibbs, J. M., Structure of the Silica/Divalent Electrolyte Interface: Molecular Insight into Charge Inversion with Increasing pH. *J. Phys. Chem. C* **2020,** *124* (49), 26973-26981.
59. Cyran, J. D.; Donovan, M. A.; Vollmer, D.; Siro Brigiano, F.; Pezzotti, S.; Galimberti, D. R.; Gaigeot, M.-P.; Bonn, M.; Backus, E. H. G., Molecular Hydrophobicity at a Macroscopically Hydrophilic Surface. *P. Natl. Acad. Sci. USA* **2019,** *116* (5), 1520.
60. Urashima, S.-h.; Uchida, T.; Yui, H., A Hydrogen-Bonding Structure in Self-Formed Nanodroplets of Water Adsorbed on Amorphous Silica Revealed via Surface-Selective Vibrational Spectroscopy. *Phys. Chem. Chem. Phys.* **2020,** *22* (46), 27031-27036.
61. Kosmulski, M., The pH Dependent Surface Charging and Points pf Zero Charge. IX. Update. *Adv. Colloid Interface Sci.* **2021,** *296*, 102519.

62. DeWalt-Kerian, E. L.; Kim, S.; Azam, M. S.; Zeng, H.; Liu, Q.; Gibbs, J. M., pH-Dependent Inversion of Hofmeister Trends in the Water Structure of the Electrical Double Layer. *J. Phys. Chem. Lett.* **2017,** *8*, 2855-2861.
63. Darlington, A. M.; Jarisz, T. A.; DeWalt-Kerian, E. L.; Roy, S.; Kim, S.; Azam, M. S.; Hore, D. K.; Gibbs, J. M., Separating the pH-Dependent Behavior of Water in the Stern and Diffuse Layers with Varying Salt Concentration. *J. Phys. Chem. C* **2017,** *121*, 20229-20241.
64. Rehl, B.; Rashwan, M.; DeWalt-Kerian, E. L.; Jarisz, T. A.; Darlington, A. M.; Hore, D. K.; Gibbs, J. M., New Insights into χ(3) Measurements: Comparing Nonresonant Second Harmonic Generation and Resonant Sum Frequency Generation at the Silica/Aqueous Electrolyte Interface. *J. Phys. Chem. C* **2019,** *123* (17), 10991-11000.
65. Doğangün, M.; Ohno, P. E.; Liang, D.; McGeachy, A. C.; Bé, A. G.; Dalchand, N.; Li, T.; Cui, Q.; Geiger, F. M., Hydrogen-Bond Networks near Supported Lipid Bilayers from Vibrational Sum Frequency Generation Experiments and Atomistic Simulations. *J. Phys. Chem. B* **2018,** *122* (18), 4870-4879.
66. Yang, P.-K.; Huang, J. Y., Phase-Retrieval Problems in Infrared–Visible Sum-Frequency Generation Spectroscopy by the Maximum-Entropy Method. *J. Opt. Soc. Am. B* **1997,** *14* (10), 2443-2448.
67. Yang, P.-K.; Huang, J. Y., Model-Independent Maximum-Entropy Method for the Analysis of Sum-Frequency Vibrational Spectroscopy. *J. Opt. Soc. Am. B* **2000,** *17* (7), 1216-1222.
68. Sovago, M.; Vartiainen, E.; Bonn, M., Determining Absolute Molecular Orientation at Interfaces: A Phase Retrieval Approach for Sum Frequency Generation Spectroscopy. *J. Phys. Chem. C* **2009,** *113* (15), 6100-6106.
69. Sovago, M.; Vartiainen, E.; Bonn, M., Observation of Buried Water Molecules in Phospholipid Membranes by Surface Sum-Frequency Generation Spectroscopy. *J. Chem. Phys.* **2009,** *131* (16), 161107.
70. de Beer, A. G. F.; Samson, J.-S.; Hua, W.; Huang, Z.; Chen, X.; Allen, H. C.; Roke, S., Direct Comparison of Phase-Sensitive Vibrational Sum Frequency Generation with Maximum Entropy Method: Case Study of Water. *J. Chem. Phys.* **2011,** *135* (22), 224701.
71. de Beer, A. G. F.; Chen, Y.; Scheu, R.; Conboy, J. C.; Roke, S., Analysis of Complex Spectra Using Fourier Filtering. *J. Phys. Chem. C* **2013,** *117* (50), 26582-26587.
72. Roy, S.; Covert, P. A.; Jarisz, T. A.; Chan, C.; Hore, D. K., Surface–Bulk Vibrational Correlation Spectroscopy. *Anal. Chem.* **2016,** *88* (9), 4682-4691.
73. Yang, W.-C.; Hore, D. K., Broadband Models and Their Consequences on Line Shape Analysis in Vibrational Sum-Frequency Spectroscopy. *J. Chem. Phys.* **2018,** *149* (17), 174703.
74. Johansson, P. K.; Koelsch, P., Vibrational Sum-Frequency Scattering for Detailed Studies of Collagen Fibers in Aqueous Environments. *J. Am. Chem. Soc.* **2014,** *136* (39), 13598-13601.
75. Hofmann, M. J.; Koelsch, P., Retrieval of Complex χ(2) Parts for Quantitative Analysis of Sum-Frequency Generation Intensity Spectra. *J. Chem. Phys.* **2015,** *143* (13), 134112.
76. Bos, A. v. d., Alternative Interpretation of Maximum Entropy Spectral Analysis. *IEEE T. Inform. Theory* **1971,** *17* (4), 493-494.
77. Myalitsin, A.; Urashima, S.; Nihonyanagi, S.; Yamaguchi, S.; Tahara, T., Water Structure at the Buried Silica/Aqueous Interface Studied by Heterodyne-Detected Vibrational Sum-Frequency Generation. *J. Phys. Chem. C* **2016,** *120* (17), 9357-9363.
78. Ohno, P. E.; Chang, H.; Spencer, A. P.; Liu, Y.; Boamah, M. D.; Wang, H.-f.; Geiger, F. M., Beyond the Gouy–Chapman Model with Heterodyne-Detected Second Harmonic Generation. *J. Phys. Chem. Lett.* **2019,** *10* (10), 2328-2334.
79. Boamah, M. D.; Ohno, P. E.; Lozier, E.; Van Ardenne, J.; Geiger, F. M., Specifics about Specific Ion Adsorption from Heterodyne-Detected Second Harmonic Generation. *J. Phys. Chem. B* **2019,** *123* (27), 5848-5856.

80. Chang, H.; Ohno, P. E.; Liu, L.; Geiger, F. M., Direct Measurement of Charge Reversal on Lipid Bilayers using Heterodyne-Detected Second Harmonic Generation Spectroscopy. *J. Phys. Chem. B* **2020,** *124* (641-9).
81. Ma, E.; Ohno, P. E.; Kim, J.; Liu, Y.; Lozier, E. H.; Miller, T. F.; Wang, H.-F.; Geiger, F. M., A New Imaginary Term in the Second-Order Nonlinear Susceptibility from Charged Interfaces. *J. Phys. Chem. Lett.* **2021,** *12* (24), 5649-5659.
82. Dalchand, N.; Dogangun, M.; Ohno, P. E.; Ma, E.; Martinson, A. B. F.; Geiger, F. M., Perturbation of Hydrogen Bonding Networks over Supported Lipid Bilayers by Poly(Allylamine Hydrochloride). *J. Phys. Chem. B* **2019,** *123* (19), 4251-4257.
83. Ostroverkhov, V.; Waychunas, G. A.; Shen, Y. R., New Information on Water Interfacial Structure Revealed by Phase-Sensitive Surface Spectroscopy. *Phys. Rev. Lett.* **2005,** *94* (4), 046102.
84. Bakker, H. J.; Skinner, J. L., Vibrational Spectroscopy as a Probe of Structure and Dynamics in Liquid Water. *Chem. Rev.* **2010,** *110*, 1498-1517.
85. Lawrence, C. P.; Skinner, J. L., Ultrafast Infrared Spectroscopy Probes Hydrogen-Bonding Dynamics in Liquid Water. *Chem. Phys. Lett.* **2003,** *369* (3), 472-477.
86. Wang, H.; Xu, Q.; Liu, Z.; Tang, Y.; Wei, G.; Shen, Y. R.; Liu, W.-T., Gate-Controlled Sum-Frequency Vibrational Spectroscopy for Probing Charged Oxide/Water Interfaces. *J. Phys. Chem. Lett.* **2019,** *10*, 5943.
87. Urashima, S.-h.; Myalitsin, A.; Nihonyanagi, S.; Tahara, T., The Topmost Water Structure at a Charged Silica/Aqueous Interface Revealed by Heterodyne-Detected Vibrational Sum Frequency Generation Spectroscopy. *J. Phys. Chem. Lett.* **2018,** *9* (14), 4109-4114.
88. Bischoff, M.; Biriukov, D.; Předota, M.; Marchioro, A., Second Harmonic Scattering Reveals Ion-Specific Effects at the SiO2 and TiO2 Nanoparticle/Aqueous Interface. *J. Phys. Chem. C* **2021,** *125* (45), 25261-25274.
89. Diot, J. L.; Joseph, J.; Martin, J. R.; Clechet, P., pH Dependence of the Si/SiO2 Interface State Density for EOS Systems: Quasi-Static and AC Conductance Methods. *J. Electroanal. Chem.* **1985,** *193*, 75-88.
90. Bousse, L.; De Rooij, N. F.; Bergveld, P., Operation of Chemically Sensitive Field-Effect Sensors As a Function of the Insulator-Electrolyte Interface. *IEEE Trans. Electron Devices* **1983,** *ED-30*, 1263-70.
91. Bard, A. J.; Faulkner, L. R., *Electrochemical Methods: Fundamentals and Applications, 2nd Edition*. John Wiley & Sons, Incorporated: 2000.
92. Habib, M. A., Solvent Dipoles at the Electrode-Solution Interface. In *Modern Aspects of Electrochemistry: No. 12*, Bockris, J. O. M.; Conway, B. E., Eds. Springer US: Boston, MA, 1977; pp 131-182.